


Dispersive tuning of intrapulse polarization

Jia Xu¹, Ari T. Friberg², and Taco D. Visser^{1,3,*} 

¹Department of Physics and Astronomy, Free University, Amsterdam, The Netherlands

²Center for Photonics Sciences, University of Eastern Finland, Joensuu, Finland

³School of Physics and Electronics, Shandong Normal University, Jinan, PR China

Received 20 February 2026 / Accepted 24 March 2026

Abstract. We show how an interferometric setup containing a polarizing beam splitter and a slab of dispersive material allows control over the evolution of the instantaneous state of polarization of an optical pulse. With this proposed method the entire Poincaré sphere can be covered by varying the material's thickness. The ability to control the state of polarization over the duration of the pulse may be useful in a wide variety of applications.

Keywords: Pulses, Polarization dynamics, Dispersion, Interferometry.

1 Introduction

Optical pulses are used in a wide range of applications such as control of chemical reactions [1], observation of electron dynamics [2], time-resolved spectroscopy [3], nonlinear microscopy [4], the generation of entangled photons [5], and quantum key distribution [6], to name but a few. The state of polarization of an optical field is a fundamental property that determines how it scatters [7] and propagates through a material medium [8]. Pulse shaping is concerned with spatio-temporal control of intensity and frequency. In addition, the ability to control the instantaneous polarization state provides another degree of freedom that can be exploited in all of the above-mentioned applications. This was examined by Gerber et al. by using an LCD inside a zero-dispersion compressor [9–11]. Here we present a theoretical analysis of an alternative method, based on optical dispersion, to manipulate the evolution of the instantaneous polarization state over the duration of the pulse.

We analyze an interferometric setup in which a polarizing beam splitter, such as a Wollaston prism, creates two orthogonally-polarized and fully correlated pulsed fields with equal amplitude, $E_x(t)$ and $E_y(t)$. Whereas one field, $E_x(t)$ say, is left unchanged, $E_y(t)$ is modified by letting it travel a distance L through a deterministic, linear, and non-absorbing dispersive medium. The two fields are then recombined to form an output pulse whose polarization evolution is found to be strongly dependent on the thickness L of the dispersive medium. As an example we study a glass-like medium. We discuss two regimes. When the thickness $L \approx 10\lambda$, the polarization evolution of the output pulse is

mainly governed by the time delay between the two pulses. When $L \approx 1000\lambda$, the polarization evolution is determined by both the time delay and the stretching of $E_y(t)$. We find that in both regimes it is possible for the instantaneous Poincaré vector to reach all points of the Poincaré sphere.

2 Plane-wave pulses

Consider a linearly-polarized pulse which is represented by an analytic signal $E(z, t)$ ([12], Sect. 3.1). Such a pulse can be expressed in terms of its spectral components by using the Fourier transform

$$E(z, t) = \int_0^\infty \tilde{E}(z, \omega) e^{-i\omega t} d\omega, \quad (1)$$

with inverse relation

$$\tilde{E}(z, \omega) = \frac{1}{2\pi} \int_{-\infty}^\infty E(z, t) e^{i\omega t} dt. \quad (2)$$

Since $E(z, t)$ is an analytic signal with $\tilde{E}(z, \omega) = 0$ if $\omega < 0$, the lower limit of integration in equation (1) is zero rather than $-\infty$. We assume that in a plane $z = 0$ the spectrum has a Gaussian shape around a center frequency ω_0 , i.e.,

$$\tilde{E}(0, \omega) = \tilde{E}_0 e^{-(\omega - \omega_0)^2 / \Omega^2}, \quad (3)$$

where \tilde{E}_0 is a constant and Ω denotes the effective width. The spectrum must be zero for negative frequencies, and also only contain optical frequencies. Together this leads to the constraint

* Corresponding author: t.d.visser@vu.nl

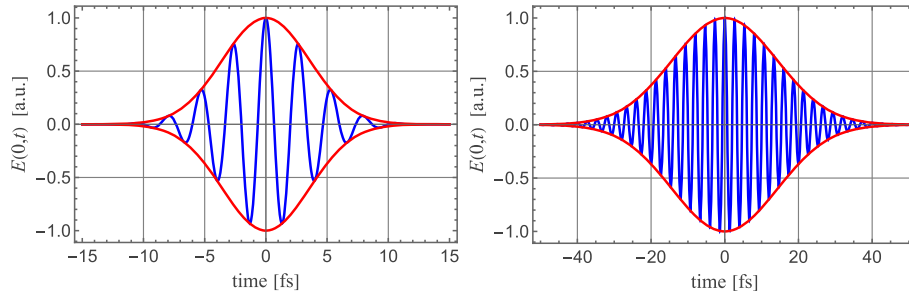


Fig. 1. Two normalized temporal pulses with center frequency $\omega_0 = 2.36 \times 10^{15}$ rad/s (corresponding to a free-space wavelength $\lambda_0 = 800$ nm) with different pulse durations T . Left: $T = 5$ fs, right: $T = 20$ fs. The envelope function $\pm A(t)$ is indicated in red. In both examples the constraint (4) is satisfied.

$$\Omega \ll \omega_0. \quad (4)$$

Let us next write the pulse as the product of an envelope function $A(t)$ and a carrier signal of frequency ω_0 :

$$E(0, t) = A(t)e^{-i\omega_0 t}. \quad (5)$$

We note that writing the pulse as an enveloped carrier signal is meaningful even at the single-cycle level [13]. To determine the envelope function we substitute from equations (3) and (5) into equation (1) to obtain

$$A(t) = \tilde{E}_0 \int_{-\infty}^{\infty} e^{-(\omega-\omega_0)^2/\Omega^2} e^{-i(\omega-\omega_0)t} d\omega \quad (6)$$

$$= \tilde{E}_0 \int_{-\infty}^{\infty} e^{-\omega'^2/\Omega^2} e^{-i\omega' t} d\omega', \quad (7)$$

where $\omega' = \omega - \omega_0$, and with the integration in equation (1) formally extended to minus infinity. This is a standard integral with solution

$$A(t) = A_0 e^{-t^2/T^2}, \quad (8)$$

where $A_0 = \tilde{E}_0 \Omega \sqrt{\pi}$, and with the pulse duration given by $T = 2/\Omega$. Using this expression for the envelope function in equation (5) gives us

$$E(0, t) = A_0 e^{-t^2/T^2} e^{-i\omega_0 t}. \quad (9)$$

The real-valued temporal pulse equals $2 \operatorname{Re}\{E(0, t)\}$, where Re denotes the real part [12].

In the optical regime the pulse duration can be on the order of femtoseconds. Examples of such temporal pulses are shown in Figure 1 for a center frequency $\omega_0 = 2.36 \times 10^{15}$ rad/s (corresponding to a free-space wavelength $\lambda_0 = 800$ nm) and $A_0 = 1/2$, for two different pulse durations. On the left is shown a few-cycle pulse and on the right a many-cycle pulse. Throughout this manuscript we will consider the latter.

3 Passage through a dispersive medium

In the interferometer sketched in Figure 2, a Wollaston prism is oriented such that it splits an incident linearly-

polarized pulse into two fully correlated orthogonally-polarized pulses with equal amplitude, denoted $E_x(t)$ and $E_y(t)$. The latter is modified by traveling a distance L through a deterministic non-absorbing, linear dispersive medium with a known refractive index profile $n(\omega)$, and is then recombined with the unchanged signal $E_x(t)$ to produce an output pulse. Fixed phase differences introduced by optical elements are not important in the present context. The path length in the upper arm can be varied, but is initially set to be the same as that in the lower arm. We study the polarization dynamics of the resulting output pulse as a function of the length L of the dispersive medium.

We take the entrance plane of the dispersive medium to be at $z = 0$. The field in this plane is, according to equation (9),

$$E_y(0, t) = A_0 e^{-t^2/T^2} e^{-i\omega_0 t}, \quad (10)$$

and therefore, from equation (3), the spectral amplitude there is

$$\tilde{E}_y(0, \omega) = \tilde{E}_0 e^{-(\omega-\omega_0)^2/\Omega^2}. \quad (11)$$

Each frequency component in equation (11) propagates with wave number $k(\omega)$ through the dispersive medium. Hence, after a distance L , the spectral amplitude becomes

$$\tilde{E}_y(L, \omega) = \tilde{E}_0 e^{-(\omega-\omega_0)^2/\Omega^2} e^{ik(\omega)L}. \quad (12)$$

We next use a Taylor expansion of $k(\omega)$ around the center frequency ω_0 and retain only quadratic terms and lower [14]

$$\tilde{E}_y(L, \omega) = \tilde{E}_0 e^{-(\omega-\omega_0)^2/\Omega^2} e^{i[kL + k'(\omega-\omega_0)L + k''(\omega-\omega_0)^2 L/2]}. \quad (13)$$

The values of k , $k' = dk/d\omega$ and $k'' = d^2k/d\omega^2$ are to be evaluated at the carrier frequency ω_0 . Substitution from equation (13) into equation (1) yields the time domain expression

$$E_y(L, t) = \tilde{E}_0 e^{ikL} \int_0^{\infty} e^{-(\omega-\omega_0)^2/\Omega^2} \times e^{i[k'(\omega-\omega_0)L + k''(\omega-\omega_0)^2 L/2]} e^{-i\omega t} d\omega. \quad (14)$$

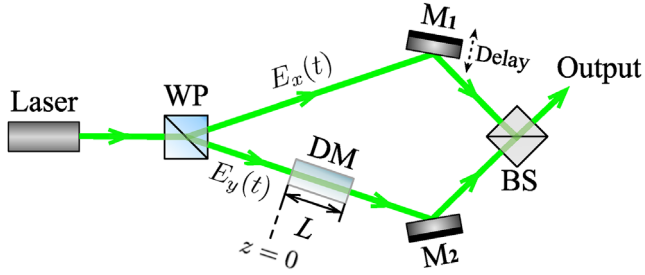


Fig. 2. Sketch of an interferometric setup to generate pulses with adjustable temporal polarization. The linearly polarized output of a pulsed laser is split into two orthogonally-polarized beams, $E_x(t)$ and $E_y(t)$, by a Wollaston prism (WP). The y -polarized beam travels a distance L through a dispersive medium (DM), and is then recombined with the pulse in the upper arm by a 50:50 beam splitter (BS) to produce the output pulse $\mathbf{E}(t)$. M_1 and M_2 are mirrors. The upper arm contains a variable free-space time delay.

Because of condition (4) we can formally extend the lower limit of integration to minus infinity and complete the square, giving us the result

$$E_y(L, t) = \tilde{E}_0 e^{ikL} e^{-i\omega_0 t} \sqrt{\pi/A} e^{-B^2/(4A)}, \quad (15)$$

where

$$A = \frac{1}{\Omega^2} - \frac{ik''L}{2}, \quad (16)$$

$$B = k'L - t, \quad (17)$$

and $\sqrt{}$ indicates the principal root. It is convenient to express the variation of the wave number k in terms of the variation of the refractive index n with the free-space wavelength λ_0 . Since $k(\omega) = n(\omega)\omega/c$, with c the speed of light in vacuum, repeated use of the chain rule yields [15]

$$k' = \frac{1}{c} \left(n - \lambda_0 \frac{dn}{d\lambda_0} \right), \quad (18)$$

$$k'' = \frac{\lambda_0^3}{2\pi c^2} \frac{d^2 n}{d\lambda_0^2}. \quad (19)$$

The values of $dn/d\lambda_0$ and $d^2n/d\lambda_0^2$ for a specific medium can be obtained from the Sellmeier dispersion model [15].

As an example we study BK7, a borosilicate optical glass, at $\lambda_0 = 800$ nm. Using its Sellmeier coefficients [16], we find that at that particular wavelength $n = 1.51078$, $dn/d\lambda_0 = -0.0198418 \mu\text{m}^{-1}$, and $d^2n/d\lambda_0^2 = 0.0492482 \mu\text{m}^{-2}$. These values correspond to $k' = 5089$ fs/mm and $k'' = 44.59$ fs²/mm. Setting the pulse width $T = 20$ fs we get, for different propagation lengths L , the electric fields shown in Figure 3. Note that for these values of L the effect of the medium is mainly to delay $E_y(t)$ with respect to $E_x(t)$. Essentially no pulse reshaping takes place.

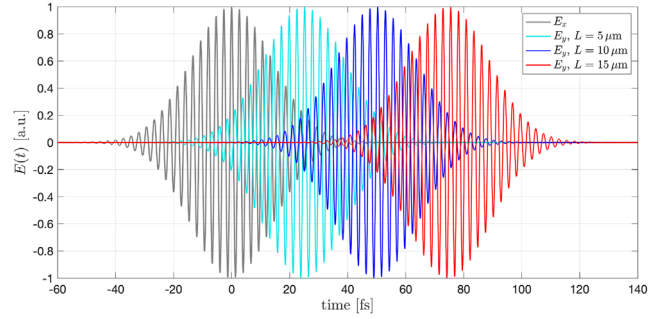


Fig. 3. Time evolution of the electric field components $E_x(t)$ and $E_y(L, t)$ of a $T = 20$ fs pulse for three selected values of the length L of the dispersive medium.

4 Instantaneous state of polarization

The conventional view of the state of polarization takes into account many cycles of the field [17], implying that the usual Stokes parameters are time-averaged quantities, and thus provide no insight into intrapulse polarization variations. Here however, we are interested in precisely such dynamics. To that end we consider a beam-like optical pulse that propagates along the z -axis. The electric field vector at time t at a point \mathbf{r} is

$$\mathbf{E}(\mathbf{r}, t) = (E_x(\mathbf{r}, t), E_y(\mathbf{r}, t)), \quad (20)$$

where $E_x(\mathbf{r}, t)$ and $E_y(\mathbf{r}, t)$ are complex analytic signal representations of the two Cartesian field components. The instantaneous Stokes parameters are defined as [18]

$$S_0(\mathbf{r}, t) = |E_x(\mathbf{r}, t)|^2 + |E_y(\mathbf{r}, t)|^2, \quad (21)$$

$$S_1(\mathbf{r}, t) = |E_x(\mathbf{r}, t)|^2 - |E_y(\mathbf{r}, t)|^2, \quad (22)$$

$$S_2(\mathbf{r}, t) = E_x^*(\mathbf{r}, t)E_y(\mathbf{r}, t) + E_y^*(\mathbf{r}, t)E_x(\mathbf{r}, t), \quad (23)$$

$$S_3(\mathbf{r}, t) = i \left[E_y^*(\mathbf{r}, t)E_x(\mathbf{r}, t) - E_x^*(\mathbf{r}, t)E_y(\mathbf{r}, t) \right], \quad (24)$$

where $*$ denotes complex conjugation. These parameters are all real-valued and it is easily verified that

$$S_0^2(\mathbf{r}, t) = S_1^2(\mathbf{r}, t) + S_2^2(\mathbf{r}, t) + S_3^2(\mathbf{r}, t). \quad (25)$$

Hence, the three normalized quantities

$$s_i(\mathbf{r}, t) = S_i(\mathbf{r}, t)/S_0(\mathbf{r}, t) \quad \text{with } i = 1, 2, 3, \quad (26)$$

constitute an instantaneous Poincaré vector

$$\mathbf{s}(\mathbf{r}, t) = (s_1(\mathbf{r}, t), s_2(\mathbf{r}, t), s_3(\mathbf{r}, t)), \quad (27)$$

whose tip is a point on the Poincaré sphere of unit radius. As the polarization state changes, this point will trace out a continuous path on the sphere. The physical significance

of instantaneous polarization is discussed in [19]. Rather than using Stokes parameters, as in the present study, there the analysis is done in terms of polarization ellipses. As explained in [17], these two approaches are equivalent. An experimental procedure to observe instantaneous polarization is described in [18].

5 Numerical results

We first analyze the case for which the path length through the dispersive medium $L \approx 10 \mu\text{m}$. The output pulse $\mathbf{E}(t) = E_x(t)\hat{\mathbf{x}} + E_y(t)\hat{\mathbf{y}}$ with, from equations (9) and (15),

$$E_x(t) = A_0 e^{-i\omega_0 t} e^{ik_0 L} e^{-t^2/T^2}, \quad (28)$$

$$E_y(t) = \frac{A_0}{\Omega\sqrt{A}} e^{-i\omega_0 t} e^{ikL} e^{-B^2/(4A)}. \quad (29)$$

The expression for $E_x(t)$ is supplemented with a phase factor $\exp(ik_0 L)$, with k_0 the free-space wave number, to ensure that the path lengths in both arms of the interferometer are identical; and with the z -dependence omitted for brevity. The instantaneous polarization of the output pulse $\mathbf{E}(t)$ changes during the duration of the pulse chiefly because of the delay of $E_y(t)$. As seen from Figure 3, the dispersive effect of the medium does not lead to any appreciable pulse stretching in this case. Because of the delay experienced by $E_y(t)$, the output pulse is initially x -polarized ($s_1 = 1$) and ends up being y -polarized ($s_1 = -1$). This is illustrated in Figure 4 where the evolution of the instantaneous Stokes parameters as well as that of the intensity are plotted for the case $L = 4 \mu\text{m}$.

During the pulse the instantaneous Poincaré vector traces out a continuous path on the Poincaré sphere between the initial state $\text{I} = (1,0,0)$ and the final state $\text{F} = (-1,0,0)$. The orientation of the path is determined by the thickness L of the dispersive medium. This is illustrated in Figure 5 for four selected values of the length L of the dispersive medium. The cyan curve ($L = 5 \mu\text{m}$) passes over the spherical quadrant ($s_2 > 0, s_3 > 0$); the blue curve ($L = 10 \mu\text{m}$) over the quadrant ($s_2 < 0, s_3 > 0$); the red curve ($L = 15 \mu\text{m}$) over the quadrant ($s_2 < 0, s_3 < 0$); and the purple curve ($L = 17 \mu\text{m}$) over the quadrant ($s_2 > 0, s_3 < 0$). Each trajectory consists of 40 steps, indicated by dots with a color gradient transitioning from blue (state I) to yellow (state F) and with a time step of 2 fs between dots (see color bar). The depicted time range is from $t = -20$ fs to $t = 60$ fs. Notice that the dot spacing is highly irregular. As illustrated in Visualization 1), as the length L is smoothly varied, so is the orientation of the path connecting states I and F, eventually covering the entire Poincaré sphere. In particular, L can be chosen such that at some moment during the pulse s_3 attains the value ± 1 .

When the thickness L of the medium exceeds $10 \mu\text{m}$, the two fields essentially no longer overlap, as is seen from Figure 3. In that case, the output field consists of two separate pulses, the first one x -polarized, and the second one y -polarized. The transition to this case is shown in Figure 6, where

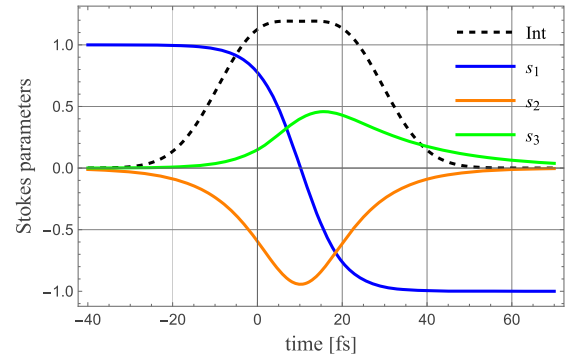


Fig. 4. Evolution of the three instantaneous Stokes parameters of the output pulse for a dispersive BK7 medium with length $L = 4 \mu\text{m}$. The input pulse duration $T = 20$ fs. The intensity (in [a.u.]) of the output pulse is represented by the dashed curve.

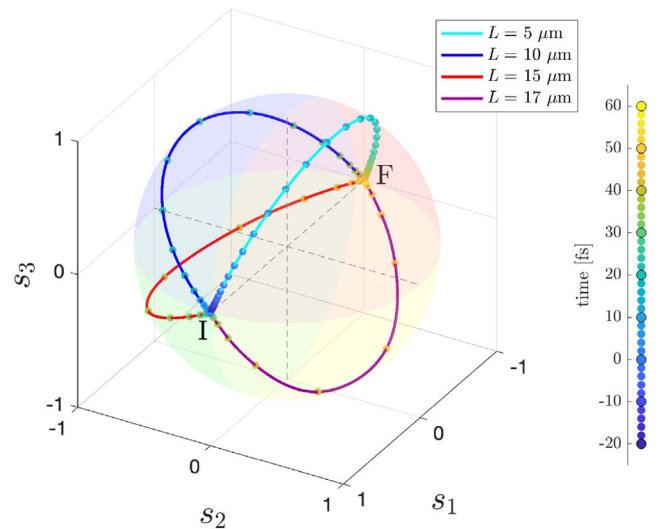


Fig. 5. Trajectories on the Poincaré sphere with axes (s_1, s_2, s_3) connecting states I (initial) and F (final), for different lengths L of the dispersive BK7 medium. Time ranges from $t = -20$ fs to $t = 60$ fs (Visualization 1).

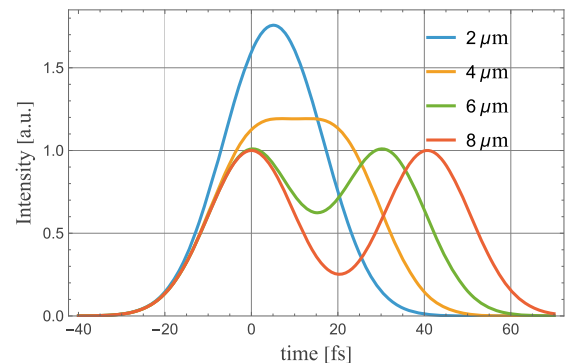


Fig. 6. The instantaneous intensity of the output pulse for four different values of the thickness of the dispersive medium.

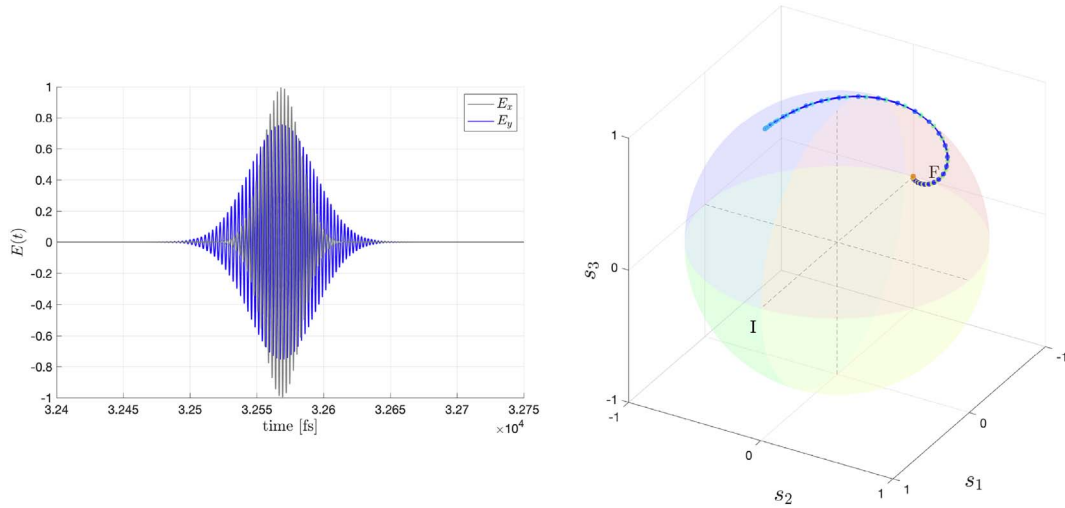


Fig. 7. Left: the $E_x(t)$ and $E_y(t)$ pulses when the former undergoes a time delay $\Delta t = k'L \approx 32568.64$ fs. Right: trajectory on the Poincaré sphere with axes (s_1, s_2, s_3) , for a length $L = 6.4$ mm of the BK7 medium. Time ranges from $t = 32500$ fs to $t = 32780$ fs with 2 fs time steps (Visualization 2).

the instantaneous intensity of the output pulse is plotted for different values of L . We note that the entire Poincaré sphere can be covered for values of L for which the field in the two arms still produces a single output pulse (see Visualization 1).

We next study the case of the same $T = 20$ fs pulse traversing a much thicker slab of the dispersive medium with $L = 6.4$ mm. The $E_y(t)$ pulse is now significantly dispersed and has stretched to about two times its original width. The $E_x(t)$ signal must be delayed by a time $\Delta t \approx k'L$ in order to overlap with the $E_y(t)$ signal. This can be achieved with the variable free-space delay line indicated in Figure 2. An example is shown in Figure 7. Here the delay is such that the two pulse peaks coincide (left panel). The result is a time-symmetric evolution of the instantaneous state of polarization. It starts out as y -polarized (state F), moves up over the upper half of the Poincaré sphere and then retraces its path back to end in state F again. In Visualization 2 both pulses and the resulting polarization trajectory of the output pulse are shown in their dependence on the time delay Δt . If $\Delta t = 32490$ fs, the E_x signal precedes E_y and the path starts at I = (1,0,0) and ends at F = (-1,0,0). When Δt is increased the path gradually twists and at around $\Delta t = 32515$ fs detaches from I. The initial state moves upward and, near $\Delta t = 32560$ fs, connects with F, forming a closed loop. Next, the path gets distorted, briefly closes (as in Fig. 7), re-opens, and gets longer and longer. Around $\Delta t = 32616$ fs the end of the path is no longer at F and begins to spiral back to state I, illustrating the richness of polarization evolutions that can be achieved with this method.

Finally, it is worth noting that these non-trivial polarization changes take place when the fields in the two arms overlap and the pulse intensity reaches its highest value. This is evidenced from Figure 8 where the instantaneous pulse intensity is shown for three different values of the time delay. The blue curve is for $\Delta t = 32568$ fs, which corresponds to the left-hand panel of Figure 7 in which the peaks

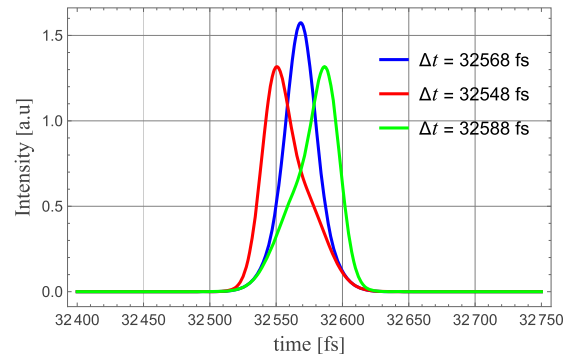


Fig. 8. The instantaneous intensity of the output pulse for three selected values of the time delay Δt of the E_x field.

of the pulses coincide. This gives rise to an output pulse with a symmetric profile. When Δt is decreased by 20 fs (red curve), or increased (green curve), the intensity profile becomes somewhat asymmetric and has a lower peak value.

6 Conclusions

We have analyzed theoretically and numerically an interferometric setup to control the instantaneous state of polarization of optical pulses. Our description is suitable for media for which third-order and higher dispersion may be neglected. Implementation-dependent issues such as phase stability and the possible use of a wedge-shaped medium to continuously vary the path length L , are not addressed.

In the proposed setup a linearly polarized pulse is split into two orthogonal and fully coherent beams. This can be achieved by a Wollaston prism or another type of polarizing beam splitter. One beam travels through free space, the other is made to propagate a distance L through a linear, non-absorbing, deterministic dispersive glass medium. The two pulses are then recombined to produce an output

pulse of which the polarization evolution is strongly influenced by the path length L . Two regimes can be distinguished. When L is just several wavelengths, the main effect of the dispersive medium is a delay between the two 20 fs pulses. In that case, the path on the Poincaré sphere, which connects an x -polarized state to a y -polarized state, has an orientation that is governed by the particular value of L . It was found that it is possible to reach any point on the Poincaré sphere in this manner. When L is on the order of 10,000 wavelengths, a time-delay for $E_x(t)$ has to be introduced in order for the pulses to overlap. Also, $E_y(t)$ becomes significantly stretched. This results in a much more complex polarization evolution of the output pulse.

One possible application of polarization-modulated pulses may be the investigation of structural changes in pump-probe experiments.

Funding

This work was supported by the Dutch Research Council (NWO), project P19-13, and the National Natural Science Foundation of China (grant W2441005).

Conflicts of interest

The authors have nothing to disclose.

Data availability statement

No data were generated in the study. Visualizations 1 and 2 are available at <https://doi.org/10.6084/m9.figshare.29828546> and <https://doi.org/10.6084/m9.figshare.30052795>.

Author contribution statement

Conceptualization: T.D.V. and A.T.F.; Methodology: J.X., T.D.V. and A.T.F.; Software: J.X. and T.D.V.; Writing – Original Draft Preparation: J.X. and T.D.V.; Writing – Review & Editing: J.X., T.D.V. and A.T.F.; Project administration: T.D.V.; Funding acquisition: T.D.V. All authors have read and agreed to the published version of the manuscript.

References

- Dey D, Tiwari AK, Controlling chemical reactions with laser pulses, *ACS Omega*. **5**, 17857–17867 (2020).
- Johnsson P et al., Attosecond electron wave packet dynamics in strong laser fields, *Phys. Rev. Lett.* **95**, 013001 (2005).
- Drescher M et al., Time-resolved atomic inner-shell spectroscopy, *Nature*. **419**, 803–807 (2002).
- Dudovich N, Oron D, Silberberg Y, Single-pulse coherently controlled nonlinear Raman spectroscopy and microscopy, *Nature*. **418**, 512–514 (2002).
- Weston MM et al., Efficient and pure femtosecond-pulse-length source of polarization-entangled photons, *Opt. Express*. **24**, 10869–10879 (2016).
- Li Y et al., Microsatellite-based real-time quantum key distribution, *Nature*. **640**, 47–54 (2025).
- Schouten HF, Visser TD, Scattering of partially coherent electromagnetic beams by a sphere, *Opt. Express*. **32**, 10690–10702 (2024).
- Lyashenko DA, Svirko YP, Crystal Optics, in: *Encyclopedia of Condensed Matter Physics*, 2nd edn., vol. **5** (Elsevier, 2024), pp. 80–87.
- Brixner T, Gerber G, Femtosecond polarization pulse shaping, *Opt. Lett.* **26**, 557–559 (2001).
- Brixner T et al., Generation and characterization of polarization-shaped femtosecond laser pulses, *Appl. Phys. B*. **74**, S133–S144 (2002).
- Brixner T et al., Adaptive shaping of femtosecond polarization profiles, *J. Opt. Soc. Am. B*. **20**, 878–881 (2003).
- Mandel L, Wolf E, *Optical Coherence and Quantum Optics*. (Cambridge University Press, 1995).
- Brabec T, Krausz F, Nonlinear optical pulse propagation in the single-cycle regime, *Phys. Rev. Lett.* **78**, 3282–3285 (1997).
- This quadratic dispersion relation is discussed in: Oughstun KE, *Electromagnetic and Optical Pulse Propagation*, vol. **2**, 2nd edn. (Springer, 2019). Sec. 11.4.2.
- Saleh BEA, Teich MC, *Fundamentals of Photonics*, 2nd edn. (Wiley, 2007). Secs. 5.5 and 5.6.
- Sellmeier coefficients taken from Schott N-BK7 Data Sheet; downloaded from www.schott.com.
- Born M, Wolf E, *Principles of Optics*, 7th edn. (Cambridge University Press, 1999).
- Brosseau C, *Fundamentals of Polarized Light* (Wiley-Interscience, 1998). Secs. 3.1.3 and 3.1.6.
- Porras MA, Propagation-induced changes in the instantaneous polarization state, phase, and carrier-envelope phase of few-cycle pulsed beams, *J. Opt. Soc. Am. B*. **30**, 1652–1659 (2013).